R-matrix method for calculating wave functions in reflection high-energy electron diffraction

T. C. Zhao* and S. Y. Tong
Department of Physics and Laboratory for Surface Studies, University of Wisconsin–Milwaukee, Milwaukee, Wisconsin 53210
(Received 23 July 1992)

We present an extension of the invariant-embedding R-matrix method for calculating wave functions in reflection high-energy electron diffraction (RHEED). Using this method, we study the strong resonances commonly observed in RHEED rocking curves. Results for an Ag(001) slab show that the resonances are associated with the trapping of diffraction beams inside planar layers and the angles at which these resonances occur can be identified by the minima in the total elastic flux. The penetration of the electron wave field inside a slab is shown to be a few monolayers deep.

I. INTRODUCTION

The diffraction of high-energy electrons (5–100 keV) in a solid has found many applications. For example, in reflection high-energy electron diffraction (RHEED), the elastically back-scattered electrons at grazing incidence to a slab are measured as a function of the incident angle (i.e., RHEED rocking curves), or atomic coverage (i.e., RHEED intensity oscillations). Proper interpretation of such data can produce structural information and understanding of the growth mode. The diffraction of high-energy electrons has also proved to be an essential component in determining image intensity, contrast, and utility in reflection electron microscopy (REM) and scanning reflection electron microscopy (SREM). In order to extract quantitative information from RHEED, REM, or SREM, it is necessary to develop an accurate and numerically stable method which describes electron diffraction in the high-energy regime. We have introduced earlier such a method: the multislice R-matrix method of RHEED.[1] In this method, a slab is sliced into small sectors parallel to the surface. Inside each sector, after proper basis transformation, a local R matrix $\mathbf{r}$ is determined by solving a square-well problem; then a global R matrix is constructed by assembling the local R matrices. An R matrix is simply the ratio of a wave function and its first derivative. After matching the boundary condition across each sector, a recursion relation for the global R matrix is obtained. The recursion starts at the bottom of the slab and propagates toward the solid-vacuum interface where the reflectivity is obtained by matching the boundary condition.

Inside a slab, a wave function may be expressed as a linear combination of basis functions with real wave numbers (i.e., propagating beams or open channels), or complex wave numbers (i.e., evanescent beams or closed channels). For propagation in a direction normal to the slab, half of the evanescent beams have amplitudes which exponentially increase while the other half have amplitudes which exponentially decrease. Earlier dynamical methods of RHEED (Refs. 2 and 3) apply the iteration process to the wave function itself. The numerical problem arises for those closed-channel basis functions which grow exponentially because their amplitudes become many orders of magnitude larger than those of the other channels. When this happens, truncation errors in the numerical process destroy the linear independence of the intermediate iterative solutions. On the other hand, the multislice R-matrix method is numerically stable because the iterative process is performed on the ratio of a wave function and its first derivative—i.e., the R matrix. This ratio does not diverge for either propagating or evanescent waves.

In this paper, we present the extension of the R-matrix RHEED method to evaluate the electron wave functions at any point in space—both inside and outside a crystal slab. The wave functions are also useful for the analysis of REM and SREM results. The layer-by-layer penetration of an electron wave function inside a slab combined with the transmission is important to the understanding of the beam-emergent resonance effect in RHEED.[4–16] In Sec. II, we present a brief review of the multislice R-matrix RHEED theory. In Sec. III, the evaluation of the transmitted wave function is given. In Sec. IV, results of layer-by-layer penetration of the wave function inside a Ag(001) slab are presented. Section V contains a summary of the results.

II. RHEED THEORY

The Schrödinger equation for electrons in a crystal potential field $V(\mathbf{r})$ is given by

$$\left[\frac{-\hbar^2}{2m}\nabla^2+V(\mathbf{r})\right]\psi(\mathbf{r})=E\psi(\mathbf{r}) . \tag{1}$$

At high energies, the scattering is dominated by a forward-direction cone around the incident beam. There, the crystal potential $V(\mathbf{r})$ and electron wave function can be expanded in a Fourier series:

$$V(\mathbf{R})=\sum_{\mathbf{g}} V_{\mathbf{g}}(z)e^{i\mathbf{g}\cdot\rho} , \tag{2a}$$

$$\psi(\mathbf{r})=e^{i\mathbf{k}_{\parallel}\cdot\rho}U(\mathbf{r}) , \tag{2b}$$

where

$$U(\mathbf{r})=\sum_{\mathbf{g}}\phi_{\mathbf{g}}(z)e^{i\mathbf{g}\cdot\rho} . \tag{2c}$$

 ©1993 The American Physical Society

Substituting Eq. (2) into Eq. (1), we obtain the following coupled second-order differential equation:

$$\phi_{\mathbf{g}}''(z)+\mathbf{k}_{\perp\mathbf{g}}^2\phi_{\mathbf{g}}(z)=\frac{2m}{\hbar^2}\sum_{\mathbf{g}'}V_{\mathbf{g}-\mathbf{g}'}(z)\phi_{\mathbf{g}'}(z)\ , \tag{3a}$$

where

$$\mathbf{k}_{\perp\mathbf{g}}^2=\frac{2mE}{\hbar^2}-(\mathbf{k}_{\parallel}+\mathbf{g})^2\ . \tag{3b}$$

In matrix form, Eq. (3) can be expressed as

$$\mathbf{\Phi}''(z)=\mathbf{W}(z)\mathbf{\Phi}(z)\ , \tag{4a}$$

where $\mathbf{\Phi}$ is a column vector

$$\mathbf{\Phi}(z)=\begin{bmatrix}\phi_{\mathbf{g}_1}(z)\\ \vdots\\ \phi_{\mathbf{g}_i}(z)\\ \vdots\\ \phi_{\mathbf{g}_N}(z)\end{bmatrix} \tag{4b}$$

and $\mathbf{W}$ is the coupling matrix

$$W_{\mathbf{g}\mathbf{g}'}=\frac{2m}{\hbar^2}V_{\mathbf{g}-\mathbf{g}'}(z)-\mathbf{k}_{\perp_g}^2\delta_{\mathbf{g}\mathbf{g}'}\ . \tag{4c}$$

In solving Eq. (4), we divided the crystal into thin slices (i.e., sectors) parallel to the surface. Inside each slice, the coupling matrix is taken to be independent of z and evaluated at the center of the slice. Since the coupling matrix is Hermitian, there exists a unitary transformation that diagonalizes it:

$$\mathbf{T}^{(i)^\dagger}\mathbf{W}^{(i)}\mathbf{T}^{(i)}=(\boldsymbol{\lambda}^{(i)})^2\ , \tag{5}$$

where $\mathbf{T}^{(i)^\dagger}$ is the Hermitian conjugate of the transformation matrix $\mathbf{T}^{(i)}$. If we define a local basis $\{\mathbf{X}\}$ as

$$\mathbf{X}^{(i)}(z)=\mathbf{T}^{(i)^\dagger}\mathbf{\Phi}^{(i)}(z) \tag{6}$$

then, in this local basis, Eq. (4) becomes decoupled. For each decoupled component, we have a simple square-well problem.

Let U and L denote the bottom (lower) and top (upper) boundaries of the sector, respectively (see Fig. 1), then it can be shown that the local wave functions at the top and bottom of the sector satisfies the following relationship:[1,17]

$$\begin{bmatrix}\mathbf{X}_L\\ \mathbf{X}_U\end{bmatrix}=\begin{bmatrix}\mathbf{r}_1 & \mathbf{r}_2\\ \mathbf{r}_3 & \mathbf{r}_4\end{bmatrix}\begin{bmatrix}-\mathbf{X}_L'\\ \mathbf{X}_U'\end{bmatrix}\ , \tag{7a}$$

where $\mathbf{r}$ are the local R matrices given by (h is the step size)

$$\begin{aligned}(\mathbf{r}_1^{(i)})_{\mathbf{g}\mathbf{g}'}&=(\mathbf{r}_4^{(i)})_{\mathbf{g}\mathbf{g}'}=\lambda_{\mathbf{g}}^{-1}\coth(\lambda_{\mathbf{g}}h)\delta_{\mathbf{g}\mathbf{g}'}\ ,\\ (\mathbf{r}_2^{(i)})_{\mathbf{g}\mathbf{g}'}&=(\mathbf{r}_3^{(i)})_{\mathbf{g}\mathbf{g}'}=\lambda_{\mathbf{g}}^{-1}\operatorname{csch}(\lambda_{\mathbf{g}}h)\delta_{\mathbf{g}\mathbf{g}'}\ .\end{aligned} \tag{7b}$$

Boundary conditions require that the wave function and its first derivative be continuous at the sector boundaries, i.e.,

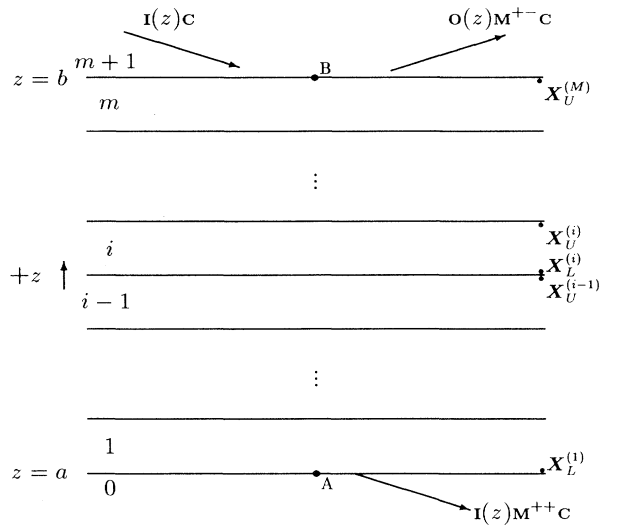

FIG. 1. Dividing a surface slab from $z=a$ to b into m slices.

$$\begin{aligned}\mathbf{X}_U^{(i-1)}&=\mathbf{Q}^{(i-1,i)}\mathbf{X}_L^{(i)}\ ,\\ \mathbf{X}_L'^{(i-1)}&=\mathbf{Q}^{(i-1,i)}\mathbf{X}_U'^{(i)}\ ,\end{aligned} \tag{8}$$

where $\mathbf{Q}^{(i-1,i)}=\mathbf{T}^{(i-1)^\dagger}\mathbf{T}^{(i)}$. In other words, the $\mathbf{Q}$ matrix takes the local basis from sector $(i-1)$ to sector (i).

The global R matrix is defined as that which always relates the wave functions and derivatives at the outer boundary of a sector, i.e.,

$$\mathbf{X}_U^{(i)}=\mathbf{R}^{(i)}\mathbf{X}_U'^{(i)}\ . \tag{9}$$

From Eqs. (7), (8), and (9), we can derive a recursion relation for the R matrix:[1]

$$\mathbf{R}^{(i)}=\mathbf{r}_4^{(i)}-r_3^{(i)}\mathbf{Z}^{(i)}\mathbf{r}_2^{(i)}\ , \tag{10a}$$

where

$$\mathbf{Z}^{(i)}=(\mathbf{r}_1^{(i)}+\mathbf{Q}^{(i-1,i)^\dagger}\mathbf{R}^{(i-1)}\mathbf{Q}^{(i-1,i)})^{-1}\ . \tag{10b}$$

III. TRANSMISSION

In the R-matrix formulation, the recursion relationship of the R matrix [Eq. (10)] is used to propagate the R matrix from the bottom of the slab, where only transmitted waves exist, to the crystal-vacuum interface. At the interface, a boundary condition is applied to obtain the reflected intensities. Since the R matrix is roughly the inverse logarithmic derivative of the local wave functions, the transmission coefficients are divided out at the beginning of the propagation, and the wave functions are not directly involved in the iteration. It is not possible to recover the transmission coefficients until the reflected intensities have been solved; therefore, it is necessary to keep track of the local wave functions in each sector. Fortunately, this bookkeeping only requires minimal effort.

From Eqs. (7) and (9), it is easy to derive the following relationship between the derivatives at the top and bot-

tom of a sector:

$$\mathbf{X}_L'^{(i)}=\mathbf{r}_3^{(i)-1}(\mathbf{r}_4^{(i)}-\mathbf{R}^{(i)})\mathbf{X}_U'^{(i)} . \tag{11}$$

By using the recursion relationship for the R matrix [Eq. (10)], Eq. (11) is simplified to

$$\mathbf{X}_L'^{(i)}=\mathbf{B}^{(i)}\mathbf{X}_U'^{(i)} , \tag{12a}$$

where

$$\mathbf{B}^{(i)}=\mathbf{Z}^{(i)}\mathbf{r}_2^{(i)} . \tag{12b}$$

Since both $\mathbf{Z}$ and $\mathbf{r}$ are available from the RHEED calculation [Eq. (10)], no extra work is required.

From Eqs. (8) and (12), we obtain a recursion relationship for the derivative:

$$\mathbf{X}_U'^{(i-1)}=\mathbf{P}^{(i-1,i)}\mathbf{X}_U'^{(i)} , \tag{13a}$$

where

$$\mathbf{P}^{(i-1,i)}=\mathbf{Q}^{(i-1,i)}\mathbf{B}^{(i)} . \tag{13b}$$

Recursive use of Eq. (13) propagates the derivative from the top of the slab, where the wave function is known from the reflection calculation, to the bottom of the slab (see Fig. 1),

$$\mathbf{X}_U'^{(1)}=\left[\prod_{i=2}^{M}\mathbf{P}^{(i-1,i)}\right]\mathbf{X}_U'^{(M)} . \tag{14}$$

The derivative at the bottom of the first sector is given by

$$\mathbf{X}_L'^{(1)}=\mathbf{B}^{(1)}\left[\prod_{i=2}^{M}\mathbf{P}^{(i-1,i)}\right]\mathbf{X}_U'^{(M)} . \tag{15}$$

In order to match the boundary conditions, we change the basis function from the local representation to the plane-wave representation; then the derivative of the wave function at the bottom of the slab just inside the solid is given by

$$\mathbf{\Phi}_L'^{(1)}=\left[\prod_{i=1}^{M}\mathbf{P}^{(i-1,i)}\right]\mathbf{T}^{(M)\dagger}\mathbf{\Phi}_U'^{(M)} . \tag{16}$$

At the top side of the slab (outside, numbered as $M+1$), there are two waves: the incident wave

$$\psi_i(\mathbf{r})=\sum_{\mathbf{g}}C_{\mathbf{g}}e^{i\mathbf{k}_{\parallel\mathbf{g}}\cdot\rho}e^{-i\mathbf{k}_{\perp\mathbf{g}}z} \tag{17a}$$

and the reflected wave

$$\psi_r(\mathbf{r})=\sum_{\mathbf{g}\mathbf{g}'}e^{i\mathbf{k}_{\parallel\mathbf{g}}\cdot\rho}e^{i\mathbf{k}_{\perp\mathbf{g}}z}M_{\mathbf{g}\mathbf{g}'}^{+-}C_{\mathbf{g}'} , \tag{17b}$$

where $\mathbf{C}$ is a column vector consisting of incident amplitude coefficients for the $\mathbf{g}$ beams and $\mathbf{M}^{+-}$ is the reflection matrix.[18,19] At the bottom of the slab, the transmitted wave can be written in terms of the transmission matrix $\mathbf{M}^{++}$ as

$$\psi_t(\mathbf{r})=\sum_{\mathbf{g}\mathbf{g}'}e^{i\mathbf{k}_{\parallel\mathbf{g}}\cdot\rho}e^{-i\mathbf{k}_{\perp\mathbf{g}}z}M_{\mathbf{g}\mathbf{g}'}^{++}C_{\mathbf{g}'} . \tag{17c}$$

Note that there is no reflection from below (see Fig. 1).

In terms of the plane-wave expansion coefficients, Eq. (17) can be rewritten as

$$\begin{aligned}\mathbf{\Phi}_i(z)&=\mathbf{I}(z)\mathbf{C} ,\\ \mathbf{\Phi}_r(z)&=\mathbf{O}(z)\mathbf{M}^{+-}\mathbf{C} ,\\ \mathbf{\Phi}_t(z)&=\mathbf{I}(z)\mathbf{M}^{++}\mathbf{C} ,\end{aligned} \tag{18}$$

where $\mathbf{I}(z)$ and $\mathbf{O}(z)$ are diagonal matrices with $e^{-i\mathbf{k}_{\perp\mathbf{g}}z}$ and $e^{i\mathbf{k}_{\perp\mathbf{g}}z}$ as the diagonal elements, respectively.

The boundary conditions yield the following equations:

$$\begin{aligned}\mathbf{\Phi}_i'(b)+\mathbf{\Phi}_r'(b)&=\mathbf{\Phi}_U'^{(M)} ,\\ \mathbf{\Phi}_t'(a)&=\mathbf{\Phi}_L'^{(1)} .\end{aligned} \tag{19}$$

Thus from Eqs. (16), (18), and (19), we obtain the transmission matrix as a function of the reflection matrix:

$$M^{++}=\mathbf{I}'^{-1}(a)\left[\prod_{i=1}^{M}\mathbf{P}^{(i-1,i)}\right]\mathbf{T}^{\dagger(M)}[\mathbf{I}'(b)+\mathbf{O}'(b)\mathbf{M}^{+-}] . \tag{20}$$

The $\mathbf{g}$th component of the transmitted wave in terms of the transmission matrix at $z\le a$ can be expressed as

$$\mathbf{\Phi}_{\mathbf{g}}^{t}(z)=I_{\mathbf{g}}(z)\mathbf{M}_{\mathbf{g}0}^{++} . \tag{21}$$

The transmitted intensity for beam $\mathbf{g}$ is therefore given by

$$\mathbf{T}_{\mathbf{g}}=\left|\frac{\mathbf{k}_{\perp\mathbf{g}}}{\mathbf{k}_{\perp 0}}\right||\mathbf{\Phi}_{\mathbf{g}}^{t}|^2 . \tag{22}$$

In this formulation, the wave function of the electron is known at any given z inside or outside the slab; therefore, its behavior can be readily analyzed. In fact, for the $\mathbf{k}$th slice, the local wave function is given by

$$\mathbf{X}_U^{(k)}=\mathbf{R}^{(k)}\left[\prod_{i=k+1}^{M}\mathbf{P}(i-1,i)\right]\mathbf{X}_U'^{(M)} . \tag{23a}$$

Or in the plane-wave representation, we have

$$\mathbf{\Phi}_U^{(k)}=\mathbf{T}^{(k)}\mathbf{R}^{(k)}\left[\prod_{i=k+1}^{M}\mathbf{P}(i-1,i)\right]\mathbf{X}_U'^{(M)} . \tag{23b}$$

Therefore, the true electron wave function for Eq. (2b) is given by

$$\psi^{(k)}(\mathbf{r})=e^{i\mathbf{k}_{\parallel}\cdot\rho}\sum_{\mathbf{g}}\phi_{\mathbf{g}}(z)e^{i\mathbf{g}\cdot\rho} . \tag{24}$$

Since the coupled equations for RHEED [Eq. (3)] include a complete set of expansion coefficients, i.e., open as well as closed channels, numerical stability becomes a concern.[1,2,20,21] Our calculations show that the current formulation is stable even when a large number of closed channels is included. The absolute values of the eigenvalues of the $\mathbf{P}$ matrix are generally smaller than unity, indicating that the error (roundoff) will not propagate or grow from one iteration to the next; instead they will die out as the calculation continues.

IV. DISCUSSION OF RESULTS

Using the above formulation, we calculate the elastically scattered flux of a six-layer Ag(001) slab at $E=20\,000$ eV. The incident direction, along the [110] azimuth, and beams included in the calculation are shown in Fig. 2. For simplicity, bulk spacings for Ag atoms are used in the slab. At this high energy, the real part of the scattering potential is well represented by the tabulation of Doyle and Turner,[22] and the imaginary part of the potential is set at 10% of the real scattering potential. No inner potential is used.[1,23] For Ag(001) at $E=20\,000$ eV, the beam-emergence conditions are determined from Eq. (3b): these are $\theta=1.7°$ for the $(0,\pm1)$ beams, $\theta=3.44°$ for the $(0,\pm2)$ beams, and $\theta=5.16°$ for the $(0,\pm3)$ beams. Using the formulation described in Sec. III, we calculate the elastic reflected and transmitted intensities of a six-layer Ag(001) slab. In Fig. 3(a), we show the total elastically reflected flux (i.e., the sum of all reflected beams); 3(b), the total elastically transmitted flux; and, in 3(c), the total elastic flux, i.e., the sum of elastically transmitted and reflected fluxes. The dashed arrows indicate the angle of beam emergence. The elastically transmitted flux [Fig. 3(b)] increases as θ_i because the scattering length decreases inside the slab like $(\sin\theta)^{-1}$. Similarly, the elastically reflected flux [3(a)] shows a broad decrease as θ_i increases. This corresponds to the fact that the scattering cone goes below the horizon as θ_i increases. The most remarkable features in the total elastic flux [3(c)] are a number of intensity minima associated with each emerging beam: the $(0,\pm2)$ beams emerge at 3.44° and the three dips associated with these beams are identified at 3.4°, 3.0°, and 2.1°. Other minima are at $\theta=0.65°$, 1.6° [associated with the $(0,\pm1)$ beams], 4.4°, 4.7°, 5.15° [associated with the $(0,\pm3)$ beams], 6.3°, and 6.6° [associated with the $(0,\pm4)$ beams].

The following is a physical explanation of the sharp minima observed in the total elastic flux: As a RHEED electron enters a solid, its amplitude can be decomposed into a number of diffracted beams. As the electron is scattered by the atomic potential, the amplitudes of these beams vary according to the scattering of the electron from one beam into another. This is the "regular

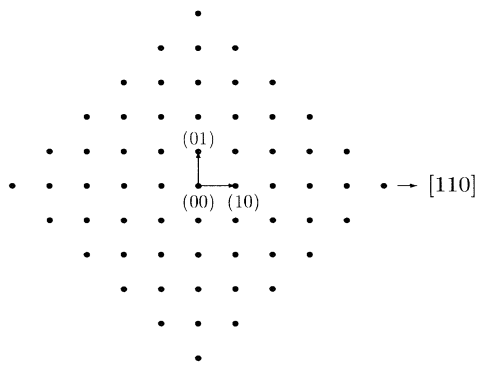

FIG. 2. Schematic diagram of the incident azimuthal direction and reciprocal space of Ag(001). The surface primitive cell convention is used.

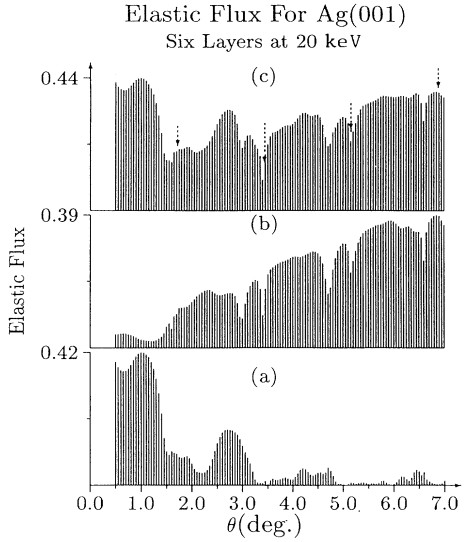

FIG. 3. Elastic flux for a six-layer slab of Ag(001) at 20 keV. (a) is the sum of reflected fluxes for all beams; (b) is the sum of the transmitted fluxes; (c) is the sum of the reflected and transmitted fluxes. Dashed arrows mark the emergence angles.

diffraction" process and it takes place at most angles. There is another process which occurs only at specific incident angles near beam-emergence conditions. This other process corresponds to having one of the beams trapped by the average potential of a linear chain of atoms parallel to the surface—in other words, this particular beam satisfies the bound-state condition of the potential for a linear chain of atoms. When such a condition is satisfied, the electron amplitude once scattered into the "bound-state" component will stay in that component for a long distance. In the presence of inelastic damping, this anomalously long scattering path along an atomic chain parallel to the surface generates an increase in the inelastic flux.[9,24] This explains why the total elastic flux in Fig. 3(c) shows sharp minima at such "bound-state" conditions. Depending on the strength of the linear-chain potential, multiple "bound states" are possible, which explains the observed minima at 3.0° and 2.1°.

At a linear-chain bound-state condition, electrons "trapped" in a given beam still have finite probabilities to scatter out of the chain and populate other beams via the regular scattering process. Furthermore, as the electron propagates into deeper layers, it might populate bound states in the deeper layers. Such a planar trapping can only occur for near-grazing angles of the incidence, e.g., the incidence direction θ measured from the surface $\leq 10°$. At larger θ, the scattering from the incident beam into a beam at emergence becomes negligible.

We investigate the penetration of the electron wave function into the successive layer at resonance. We choose as examples $\theta=3.0°$ and 3.4° (measured from the surface), which correspond to the two resonance conditions associated with the $(0,\pm2)$ beams. In Fig. 4, the amplitude squared of the (02) beam [or the equivalent $(0\bar{2})$ beam] $[|\phi_{02}(z)|^2]$ in a range of angles near 3.0° and 3.4° is plotted as a function of depth (z) inside the solid. We ob-

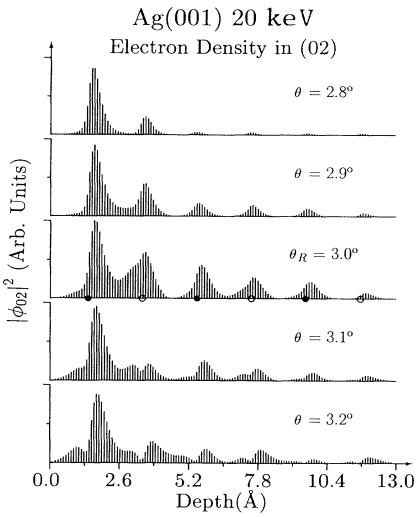

FIG. 4. Electron density as a function of depth for the (02) beam. $\theta=3°$ corresponds to a local minimum in the total elastic flux in Fig. 3(c). Depth is a line normal to the surface and it passes through the Ag nuclei (solid circle) in layers 1, 3, and 5. Open circles indicate Ag nuclei in layers 2, 4, and 6 projected onto this line.

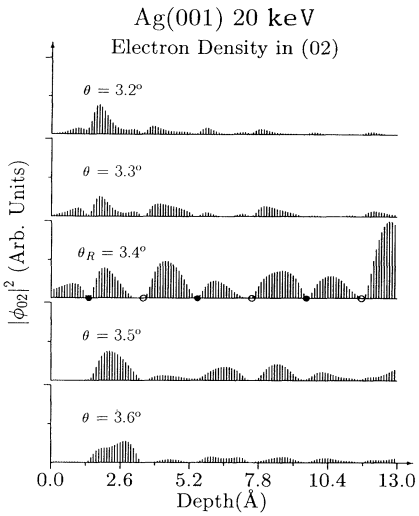

FIG. 5. Same as in Fig. 4 except for $\theta=3.40°$.

serve that in both figures there is an increase in the electron flux of the (02) beam at the resonance angles $\theta_R=3.0°$ and 3.4°, respectively. This confirms the "trapping picture." Also, we observe that the amplitude (squared) of the (02) beam peaks at the Ag nuclei (solid and open circles) at $\theta_R=3.0°$ and is zero at the Ag nuclei at $\theta_R=3.4°$. This resembles an even and odd parity of a bound-state wave function.[11] Furthermore, both cases demonstrate that the linear-chain trapping is not confined to the first atomic layer only, because at $\theta_R=3.0°$ trapping is evident for at least three atomic layers while at $\theta_R=3.4°$ trapping is evident for all six layers of the slab. At no incident angle does the electron wave field vanish behind the first atomic layer, as suggested in earlier works.[12,15,25]

The multilayer penetration of the electron beam at resonance also explains why, historically, one associates bound-state conditions with intensity anomalies in which there are sharp increases in the inelastic electrons.[9,24] It is clear from Figs. 4 and 5 that, at resonance, the (02) beam is trapped in a number of atomic layers. The total distance traveled by the electron inside the slab is thus increased, resulting in an anomalously large amount of inelastic excitations.[24,25]

V. SUMMARY

We have extended the R-matrix method to include the evaluation of transmission coefficients as well as the electron wave function at any point in space—both inside and outside a crystal slab. Using this new formulation, we find that resonance conditions correspond to the trapping of an electron's wave-field "bound states" of a linear chain of atoms parallel to the surface. The resonances are marked by sharp minima in the total elastic flux of an ultrathin slab (≤ 10 monolayers). The penetration of the electron wave field at resonance is deep—it does not vanish behind the first atomic layer. The effects of the bound-state resonance on rocking curves and intensity oscillations will be presented elsewhere.[16,26]

ACKNOWLEDGMENTS

This work was supported by the National Science Foundation, Grant No. DMR-8805938 and NASA. The computation was carried out at the Illinois National Center for Supercomputing Applications (NCSA) and NASA Ames.

*Also at Physics Department and Space Vacuum Epitaxy Center, University of Houston, Houston, TX 77204-5504.

[1]T. C. Zhao, H. C. Poon, and S. Y. Tong, Phys. Rev. B **38**, 1172 (1988).
[2]P. A. Maksym and J. L. Beeby, Surf. Sci. **110**, 423 (1981).
[3]A. Ichimiya, Jpn, J. Appl. Phys. **22**, 176 (1983).
[4]S. Kikuchi and S. Nakagawa, Sci. Papers Inst. Phys. Res. Tokyo **21**, 251 (1933).
[5]S. Miyake, K. Kohra, and S. Takagi, Acta. Crystallogr. A **7**, 393 (1954).
[6]S. Miyake and K. Hayakawa, Acta. Crystallogr. A **26**, 60 (1970).
[7]K. Komaki and F. Fijimoto, Phys. Lett. A **49**, 445 (1974).
[8]K. Hayakawa and S. Miyaki, Acta Crystallogr. A **30**, 374 (1974).
[9]Y. Horio and A. Ichimiya, Physica **117B/118B**, 792 (1983).
[10]A. Ichimiya and G. Lehmpfuhl, Z. Naturforsch. A **33**, 269 (1978).

[11]K. Kambe, G. Lehmpfuhl, and F. Fujimoto, Z. Naturforsch. A **29**, 1033 (1974).
[12]P. A. Maksym and J. L. Beeby, Surf. Sci. **11/12**, 663 (1982).
[13]L.-M. Peng and J. M. Cowley, Surf. Sci. **201**, 559 (1988).
[14]T. C. Zhao and S. Y. Tong, Ultramicroscopy **26**, 151 (1988).
[15]H. Martin and G. Meyer-Ehmsen, Surf. Sci. **151**, 570 (1985).
[16]T. C. Zhao and S. Y. Tong (unpublished).
[17]S. Y. Tong, T. C. Zhao, and H. C. Poon, in *RHEED and Reflection Electron Imaging of Surfaces,* edited by P. K. Larsen and P. J. Dobson (Plenum, New York, 1988).
[18]S. Y. Tong, Prog. Surf. Sci. **7**, 1 (1975).
[19]M. A. Van Hove and S. Y. Tong, *Surface Crystallography by LEED* (Springer, Berlin, 1979).
[20]T. Kawamura, A. Ichimiya, and P. A. Maksym, Jpn. J. Appl. Phys. **27**, 1098 (1988).
[21]G. Meyer-Ehmsen, Surf. Sci. **219**, 177 (1990).
[22]P. A. Doyle and P. S. Turner, Acta Crystallogr. A **24**, 390 (1968).
[23]S. Y. Tong, T. C. Zhao, H. C. Poon, K. D. Jamison, D. N. Zhou, and P. I. Cohen, Phys. Lett. A **128**, 447 (1988).
[24]A. Ichimiya and Y. Takeuchi, Surf. Sci. **128**, 343 (1983).
[25]G. Meyer-Ehmsen, in *Rheed and Reflection Electron Imaging of Surfaces,* edited by P. K. Larsen and P. J. Dobson (Plenum, New York, 1988).
[26]J. U. Andersen, K. R. Eriksen, and E. lægsgaard, Phys. Scr. **24**, 588 (1981).
[27]T. C. Zhao and S. Y. Tong (unpublished).